

## STATISTICAL EVIDENCE FOR THREE CLASSES OF GAMMA-RAY BURSTS

TANUKA CHATTOPADHYAY<sup>1</sup>, RANJEEV MISRA<sup>2</sup>, ASIS KUMAR CHATTOPADHYAY<sup>3</sup> AND MALAY NASKAR<sup>4</sup>  
*Draft version October 29, 2018*

### ABSTRACT

Two different multivariate clustering techniques, the K-means partitioning method and the Dirichlet process of mixture modeling, have been applied to the BATSE Gamma-ray burst (GRB) catalog, to obtain the optimum number of coherent groups. In the standard paradigm, GRB are classified in only two groups, the long and short bursts. However, for both the clustering techniques, the optimal number of classes was found to be three, a result which is consistent with previous statistical analysis. In this classification, the long bursts are further divided into two groups which are primarily differentiated by their total fluence and duration and hence are named low and high fluence GRB. Analysis of GRB with known red-shifts and spectral parameters suggests that low fluence GRB have nearly constant isotropic energy output of  $10^{52}$  ergs while for the high fluence ones, the energy output ranges from  $10^{52}$  to  $10^{54}$  ergs. It is speculated that the three kinds of GRBs reflect three different origins: mergers of neutron star systems, mergers between white dwarfs and neutron stars, and collapse of massive stars

*Subject headings:* Gamma Rays: Bursts - Methods: Data Analysis - Methods: Statistical

### 1. INTRODUCTION

Although it has now been well established that Gamma-Ray Bursts (GRB) are of cosmological origin, their nature and source still remains a mystery. Detailed observations and studies of their afterglow emission have revealed important information regarding the dynamic features and environments of these explosive events (see Piran (2005) for a review). The detection of supernova light curve in the afterglows of long duration nearby GRB has indicated that a fraction of the GRB occur during the the collapse of a massive star (see Woosley & Bloom (2006) for a review). Other mechanism that could produce GRB are the merger of compact objects like a pair of neutron stars or a neutron star with a black hole (e.g. Piran 1992; Gehrels et al. 2005; Bloom et al. 2006). Thus GRB may be a heterogeneous group and a proper classification of the phenomena is crucial to isolate and identify the possible different sources. Such a classification will also enable the identification of spectral or temporal correlations which may exist only for a particular class of GRB.

In general, GRB have been classified into two groups of long ( $> 2$  sec) and short ( $< 2$  sec) duration bursts. This is based on visual inspection of the distribution of burst duration which clearly shows two peaks. Theoretically, this may be understood by identifying long bursts with collapsing stars where the duration of the event is linked to the dynamical collapse time-scale. On the other hand, the merger of two neutron stars should occur on short timescales and hence may correspond to the short duration bursts. In this scenario, the long duration bursts should always be associated with a supernova explosion and occur in star burst regions, while short bursts should have no relation to star burst regions and should have no associated supernova. However, theoretically another mechanism to create a GRB could be the merger of

neutron stars with white dwarfs. These would be long duration bursts, with no associated supernova and could be a significant fraction of the total observed bursts (King et al. 2007). Observationally, there have been some evidence that there may be more than two classes of GRB. Some GRB have been recorded with low intrinsic luminosity and do not comply with standard spectral relationships (Sazonov et al. 2004; Soderberg et al. 2004). More compelling evidence was the absence of a super-nova light curve in two nearby bursts, GRB 060614 and 060505, which suggested that not all long duration bursts are due to massive stellar collapses (Gehrels et al. 2006; Fynbo et al. 2006), although for GRB 060614 this result has been disputed by Schaefer & Xiao (2006), who claim that this GRB is not a nearby one. While confirmation of these results are awaited, they do highlight the need to examine the possibility that there are more than two types of GRB.

The Burst and Transient Source Experiment (BATSE) on board the COMPTON Gamma-Ray Observatory (CGRO) has provided spectral and temporal information for more than 1500 GRB. Although BATSE provides several spectral parameters, the bimodal distribution of GRB is based on univariate analysis i.e. only duration is considered as a parameter (e.g. Dezalay et al. 1992; Kouveliotou et al. 1993). There is a claim that even such a univariate analysis supports the existence of three classes (Horváth 1998). Classification analysis taking into account more observed parameters, i.e. a multivariate analysis, was first undertaken by Feigelson & Babu (1998). Subsequently, different type of analysis were undertaken to classify GRB. Baumgart (1994) used a neural network technique while Bagoly et al. (1998) have undertaken a factor analysis. Nonparametric hierarchical clustering techniques have been used by Mukherjee et al. (1998) for 797 GRB with six variables and by Balastegui et al. (2001) for 1599 GRB with nine variables. The results were confirmed for the complete BATSE GRB catalog (Horváth 2002). Hakkila et al. (2003) used a unsupervised pattern recognition algorithm while Horváth et al. (2006) have classified GRB by fitting bivariate distributions to the observed duration and hardness ratios. In all these cases, the authors have claimed the existence of at least three classes of GRB

<sup>1</sup> Shibpur Dinobundhoo College, 412/1 G.T. Road (South), Howrah 711102, India. Email: tanuka@iucaa.ernet.in

<sup>2</sup> Inter-University Centre for Astronomy and Astrophysics, Post Bag 4, Ganeshkhind, Pune 411007. Email: rmisra@iucaa.ernet.in

<sup>3</sup> Department of Statistics, Calcutta University, 35 Ballygunge Circular Road, Kolkata 700019, India. Email: akcstat@caluniv.ac.in

<sup>4</sup> NIRJAIT, Indian Council of Agricultural Research, 12, Regent Park, Kolkata 700 040, India. Email: malaynaskar@yahoo.com

although it is not clear whether the different classifications found are consistent with each other, primarily because of the different techniques and the choice of different observed parameters and data sets.

These analyses are based on the observed properties of the GRB and are hence subject to observational biases. In fact, Hakkila et al. (2000) argue that such classification techniques are significantly hampered and the three classes found is probably due to such biases (see Horváth et al. (2006) for a counter argument). Indeed, a proper classification should be based on intrinsic rather than observed properties. However since the number of GRB with known red-shift and uniformly measured temporal and spectral parameters is small, such an exercise is presently not possible. Although it can be argued that certain correlations between observed parameters (e.g. the positive correlation between duration and flux) cannot be entirely due to observational bias, it is difficult to ascertain whether the quantitative relationships are not affected. A prudent approach may be to treat such classification as indicative of the nature of systems which should be corroborated by theoretical expectations and further observations. Since theoretical expectations are on intrinsic properties, there is a need to estimate how these intrinsic properties cluster, given the results of a classification based on observed ones. The classification itself should be tested for robustness using different types of schemes. The result of such an analysis may guide or be supported by theoretical models. Moreover, the results can lay down the broad framework and requirements of future observations which can confirm or rule out the proposed theoretical scenario.

In this work, we use two different multivariate clustering techniques, the K-means partitioning method and the Dirichlet process of mixture modeling, to classify GRB based on their observed properties. These two schemes, which have not been used before for GRB, have the advantage that they do not follow any prior assumption about the number of homogeneous classes. The optimum classification comes out of the process itself. The two schemes allow for post classification discriminant analysis which can be used to verify the acceptability of the classification by computing classification/misclassification probabilities. More importantly, a GRB which is not in the original sample and which has only a subset of the observed properties used for the classification can be assigned a probability for it to be a member of a certain class. Thus although our analysis has been based on the BATSE catalog, GRB with known red-shifts (which have been observed by other instruments) can be assigned such probabilities and suitably classified. As we shall see, this not only provides qualitative estimation of any possible observational bias, but can constrain the intrinsic properties of the different clusters. We have selected 21 GRB with known redshifts and well constrained spectral parameters for such classifications and obtained constraints on the cluster's average luminosity.

In the next section, we briefly describe the two classification schemes and present the result of the analysis on the BATSE catalog. In §3, the classification obtained from the BATSE data are used to classify GRB with known red-shifts and inferences are made on the intrinsic properties of the different GRB groups. In §4 the work is summarized and the main results are discussed.

## 2. CLUSTERING ANALYSIS FOR GRB DATA

The BATSE catalog provides temporal and spectral information for more than 1500 GRB. The parameters include,

two measures of burst durations, the times within which 50% ( $T_{50}$ ) and 90% ( $T_{90}$ ) of the flux arrive, three peak fluxes,  $P_{64}, P_{256}, P_{1024}$  measured in 64, 256 and 1024 ms bins respectively, four time integrated fluences  $F_1 - F_4$ , in the 20–50, 50–100, 100–300 and > 300 KeV spectral channels. Many of the parameters are highly correlated and following previous works (e.g. Mukherjee et al. 1998; Hakkila et al. 2000) we use the following six parameter set:  $\log T_{50}, \log T_{90}, \log P_{256}, \log F_T, \log H_{32}, \log H_{321}$ , where  $F_T = F_1 + F_2 + F_3 + F_4$  is the total fluence while  $H_{32} = F_3/F_2$  and  $H_{321} = F_3/(F_1 + F_2)$  are measures of spectral hardness. The sample consists of 1594 GRB that have non-zero detections of these parameters. We have not introduced any completeness criteria (like a lower flux cutoff), since incompleteness primarily affects the short duration bursts and hence is not expected to change the qualitative results obtained. We retain the  $F_4$  flux (in the definition of  $F_T$ ), despite the uncertainties in its calibration and sensitivity, because as we discuss later in §4, the  $\gamma$ -ray flux > 300 keV is expected to have important spectral information. However, this fluence is not used in the computation of spectral hardness.

### 2.1. Partitioning (K-means clustering) method

Over the last several decades, different algorithms have been developed for Cluster Analysis which is used to find groups in a multivariate data set. The choice of a clustering algorithm depends both on the type of data available and on the particular purpose. Generally, clustering algorithms can be divided into two principal types viz. partitioning and hierarchical methods. A partitioning method constructs K clusters i.e. it classifies the data into K groups which together satisfy the requirement of a partition such that each group must contain at least one object and each object must belong to exactly one group. So there are at most as many groups as there are objects ( $K \leq n$ ). Two different clusters cannot have any object in common and the K groups together add up to the full data set. The aim is usually to uncover a structure that is already present in the data. On the other hand, Hierarchical algorithms do not construct single partition with K clusters but they deal with all values of K in the same run. The extreme partitions with  $K = 1$  (all objects are together in one cluster) and  $K = n$  (where each object forms a separate cluster) is a part of the output. In between all values of  $K = 2, 3, \dots, n-1$  are covered in a kind of gradual transition. The only difference between  $K = r$  &  $K = r+1$  is that one of the  $r$  clusters splits in order to obtain  $r+1$  clusters or two of the  $(r+1)$  clusters combined to yield  $r$  clusters. In this method either one starts with  $K = n$  and move hierarchically downwards where at each step two clusters are merged depending on similarity until only one is left i.e.  $K = 1$  (agglomerative) or the reverse way where one starts with  $K = 1$  and moves upwards where at each step one cluster is divided into two (depending on dissimilarity) until  $K = n$  (divisive). Most of the previous works on GRB (e.g. Mukherjee et al. 1998; Hakkila et al. 2000; Balastegui et al. 2001) have been based on hierarchical clustering. However, for GRB classification, a partitioning method may be more applicable because (a) it tries to select the best clustering with K groups which is not the goal of a hierarchical method, (b) a hierarchical method can never repair what was done in previous steps and (c) partitioning methods are designed to group items rather than variables into a collection of K clusters.

In this work, we apply the K-means method of MacQueen (1967) which is probably the most widely technique, to the

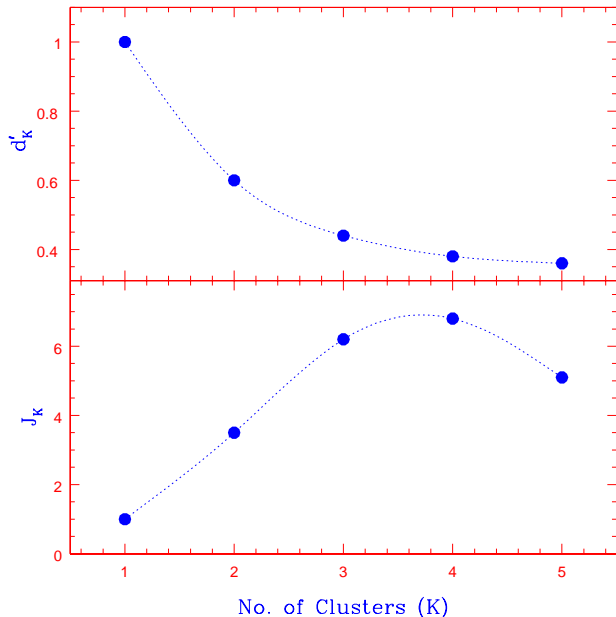


FIG. 1.— The distortion curve  $d'_K$  and the transformed jump curve  $J_K$  for different number of clusters. The largest value of  $J_K$  and the leveling of  $d'_K$  indicates that for the K-means clustering technique the optimal number of clusters is three.

BATSE catalog. For this method, the optimum value of  $K$  can be obtained in different ways (Hartigan 1975). This is done by computing for each cluster formation (i.e. for number of clusters  $K = 2, 3, 4, \dots$ ) a distance measure  $d_K = (1/p) \min_x E[(x_K - c_K)^2]$  which is defined as the distance of the  $x_K$  vector (values of the parameters) from the center of a cluster  $c_K$  (which is estimated as mean value).  $p$  is the order of the  $x_K$  vector, i.e. the number of parameters which for our case is six. If  $d'_K$  is the estimate of  $d_K$  at the  $K^{\text{th}}$  point, then  $d'_K$  is the minimum achievable distortion associated with fitting  $K$  centers to the data. A natural way of choosing the number of clusters is to plot  $d'_K$  versus  $K$  and look for the resulting distortion curve. This curve will monotonically decrease with increasing  $K$ , till  $K$  is greater than true number of clusters, after which the curve will level off with a smaller slope. This is expected since adding more clusters beyond the true number, will simply create partitions within a group. According to Sugar & James (2003) it is more illustrative to consider the transformation of the distortion curve to an appropriate negative power,  $J_K = (d'_K)^{-(p/2)} - d'_{K-1}$ , which will exhibit a sharp "jump" when  $K$  equals the true number of clusters. The optimum number of clusters is the value of  $K$  at which the distortion curve levels off as well as its value associated with the largest jump for the transformed curve.

Fig 1 shows the distortion curve and transformed jump curve for the analysis of the BATSE data. The leveling of the distortion curve and the shape of the jump function strongly suggests that the optimum number of clusters is greater than two and is likely to be three. The group means and the standard errors for the six parameters for three cluster classification, are tabulated in Table 1. Cluster I with 423 members has an average  $\langle T_{90} \rangle \sim 0.5$  s can be clearly identified with the short duration bursts. The long duration bursts are cleanly separated into two clusters (clusters 2 and 3) with 622 and 549

TABLE 1  
AVERAGE CLUSTER PROPERTIES BASED ON K-MEANS CLASSIFICATION

Parameters	Cluster I	Cluster II	Cluster III
$T_{50}$ (sec)	$0.19 \pm 0.01$	$5.37 \pm 0.25$	$22.9 \pm 1.0$
$T_{90}$ (sec)	$0.50 \pm 0.02$	$15.85 \pm 0.73$	$63.1 \pm 2.9$
$P_{256}$ (#/cm <sup>2</sup> /sec)	$1.66 \pm 0.08$	$1.26 \pm 0.06$	$2.88 \pm 0.13$
$F_T$ ( $\times 10^{-6}$ ergs/sec)	$0.62 \pm 0.04$	$2.34 \pm 0.11$	$17.8 \pm 0.8$
$H_{32}$	$5.50 \pm 0.13$	$2.45 \pm 0.06$	$3.16 \pm 0.07$
$H_{321}$	$3.39 \pm 0.08$	$1.32 \pm 0.03$	$1.78 \pm 0.04$

NOTE. — Errors quoted are standard errors. The number of members are 423, 622 and 549 for Clusters I, II and III respectively.

TABLE 2  
DISCRIMINANT ANALYSIS FOR THE K-MEANS CLASSIFICATION

	Cluster I	Cluster II	Cluster III
Cluster I*	417	28	0
Cluster II*	6	578	23
Cluster III*	0	21	526
Total	423	622	549

NOTE. — Clusters I, II and III, are the clusters obtained from the K-means classification. Clusters I\*, II\* and III\* are the clusters to which the GRB were assigned by the Discriminant analysis.

members.

Once the optimum classification (clustering) is obtained, using a process called Discrimination Analysis Johnson (1996), one can verify the acceptability of the classification by computing classification/misclassification probabilities for the different GRB. Although the K-means clustering method is purely a data analytic method, for classification it may be necessary to assume that the underlying distribution is Multivariate Normal. In this standard procedure, using the probability density functions in parameter space for the different clusters, one can assign an object (in this case a GRB) to be a member of a certain class. If the original classification was robust, then every GRB should be classified again as a member of the same class that it was before. If a significant number of objects are not reclassified then that would mean that the original classification was not stable and hence not trustworthy. Table 2 show the result of a Discrimination Analysis, where the columns represent how the GRB of a cluster were assigned by the analysis. The fraction of correct classification is 0.954 which implies that the classification is indeed robust.

## 2.2. Dirichlet process model based clustering

The standard approach to model-based clustering analysis, is based on modeling by finite mixture of parametric distributions. For example, Mukherjee et al. (1998) used such a model based approach to analyze GRB data where they assumed that the GRB population consists of mixture of multivariate Gaussian classes. The number of classes is, however, determined from an initial classification method (e.g. via agglomerative hierarchical clustering). The Dirichlet process model based clustering is more general and avoids the assumption of known number of possible classes. Since this method is less commonly used as compared to the K-means

technique, we describe here the basic concept on the analysis in more detail.

The Dirichlet process avoids a prior assumption of the number of classes by applying a Bayesian non-parametric modeling of the unknown distribution for the multi component data. In this particular case the six component GRB data can be represented by  $x_i = (\log T_{50}, \log T_{90}, \log F_T, \log P_{256}, \log H_{321}, \log H_{32})^t, i = 1, 2, \dots, n$ . More specifically,  $x_i$  is assumed to follow a multivariate normal distribution whose mean vector is generated from a Dirichlet Process (DP). Following Escobar & West (1995), the method is best conceptualized by representing the model as

$$x_i | \mu_i, \Sigma \sim \text{MVN}(\mu_i, \Sigma), \quad i = 1, 2, \dots, n; \\ \mu_i | G \sim G; \quad G \sim \text{DP}(\alpha G_0) \quad (1)$$

where MVN means multivariate normal distribution,  $G$  is a discrete measure of the unknown distribution,  $\alpha$  is the precision parameter and  $G_0$  is a known base measure distribution. Since  $G$  is discrete, there can be ties among the  $\mu_i$ 's, which can also be seen from polya urn representation of Blackwell & MacQueen (1973) as

$$\mu_i | \mu_1, \mu_2, \dots, \mu_{i-1} \sim \frac{\alpha}{\alpha + i - 1} G_0 + \frac{1}{\alpha + i - 1} \sum_{h=1}^{i-1} \delta(\mu_h) \quad (2)$$

where  $\delta(x)$  is the distribution concentrated at the single point  $x$ . It is evident from Eqn. (2) that  $\mu_i$  are marginally sampled from  $G_0$  with positive probability and that some of the  $\mu_i$ 's are identical. Thus, a partition of  $S = \{1, 2, \dots, n\}$  can be formed by defining classes under the relation that  $\mu_i$  belongs to the  $j^{\text{th}}$  class if and only if  $\mu_i = \mu_j, j = 1, 2, \dots, k$ ,  $k$  being the number of distinct  $\mu_i$ 's,  $i = 1, 2, \dots, n$ . This induces a certain posterior distribution of  $S$  and a posterior inference can then be used to provide clustering procedure. There are various algorithms available to obtain the posterior partitions of  $S$  which are useful for making inferences on clustering of  $x_1, x_2, \dots, x_n$ . We implement the independent and identically distributed Weighted Chinese Restaurant (iidWCR) algorithm (see Ishwaran & Takahara 2002) which comes from its use of the partition distribution of  $S$ . Let  $p = \{C_1, C_2, \dots, C_{n(p)}\}$  be a partition of size  $n(p)$  of  $S$ , where each  $C_j$  contains  $e_j$  elements. Assuming  $G_0$  as the multivariate normal with mean vector  $m$  and covariance matrix  $B_0$  and denoting  $N_p(x; \mu, \Sigma) = (2\pi)^{-\frac{n}{2}} |\Sigma|^{-\frac{1}{2}} \exp[-\frac{1}{2}(x - \mu)' \Sigma^{-1}(x - \mu)]$  as the density of a  $p$ -component multivariate normal distribution, the iidWCR algorithm for inducing posterior partition of  $S$  consists of following steps:

**Step 1:** Assign  $p_1 = \{1\}$  and the corresponding importance weight  $\lambda(1) = N_6(x_1; m, \Sigma_0 + B_0)$  where  $\Sigma_0$  is the initial estimate of  $\Sigma$ .

**Step  $r$ :** Given  $p_{r-1}$ , compute  $\Sigma_{r-1}$  from  $x_1, x_2, \dots, x_{r-1}$ . Create  $p_r$  by assigning label  $r$  to a new set with probability  $\frac{\alpha}{(\alpha+r-1)\lambda(r)} \times N_6(x_r; m, \Sigma_{r-1} + B_0)$ . Otherwise, assign label  $r$  to an existing set  $C_{j,r-1}$  with probability  $\frac{e_{j,r-1}}{(\alpha+r-1)\lambda(r)} \times N_6(x_r; \mu_{j,r-1}, \Sigma_{j,r-1})$  where  $\Sigma_{j,r-1} = (B_0^{-1} + e_{j,r-1} \Sigma_{r-1}^{-1})^{-1}$  and  $\mu_{j,r-1} = \Sigma_{j,r-1} (B_0^{-1} + e_{j,r-1} \Sigma_{r-1}^{-1})^{-1} \bar{x}_{j,r-1}$ . Note that  $e_{j,r-1}$  and  $\bar{x}_{j,r-1}$  are the number of elements and observed mean in  $C_{j,r-1}$  respectively and  $\lambda(r)$  is the normalizing constant.

TABLE 3  
AVERAGE CLUSTER PROPERTIES BASED ON THE DIRICHLET MIXTURE MODELING METHOD

Parameters	Cluster I	Cluster II	Cluster III
$T_{50}$ (sec)	$0.31 \pm 0.02$	$6.76 \pm 0.31$	$16.22 \pm 1.50$
$T_{90}$ (sec)	$0.45 \pm 0.03$	$19.05 \pm 0.88$	$43.65 \pm 3.02$
$P_{256}$ (#/cm <sup>2</sup> /sec)	$1.66 \pm 0.08$	$1.35 \pm 0.03$	$4.79 \pm 0.33$
$F_T$ ( $\times 10^{-6}$ ergs/sec)	$0.89 \pm 0.06$	$3.46 \pm 0.08$	$18.2 \pm 0.2$
$H_{32}$	$4.68 \pm 0.22$	$2.82 \pm 0.06$	$3.31 \pm 0.15$
$H_{321}$	$2.75 \pm 0.13$	$1.58 \pm 0.04$	$1.86 \pm 0.09$

NOTE. — Errors quoted are standard errors. The number of members are 409, 892 and 293 for Clusters I, II and III respectively.

Running step 1 followed by step  $r$  for  $r = 2, 3, \dots, n$  gives a draw from posterior partition of  $S$ . This  $n$ -step draw, in fact, provides an iid sample from WCR density given by

$$g(p) = \frac{f(x|p)\pi(p)}{\Delta(p)} \quad (3)$$

where  $\pi(p)$  is the prior density of  $p$ ,  $f(\cdot)$  is the density of  $x$  and  $\Delta(p) = \lambda(1) \times \lambda(2) \times \dots \times \lambda(n)$  is the importance weight. Repeating the above algorithm  $B$  times, one can obtain  $p^1, p^2, \dots, p^B$  iid sample observations from posterior partition of  $S$ . Based on these sample observations, Monte Carlo method can be devised to estimate  $E\{n(p)\}$ , the expected number of clusters, as

$$E\{\widehat{n(p)}\} \approx \frac{\sum_{b=1}^B n(p^b) \Delta(p^b)}{\sum_{b=1}^B \Delta(p^b)} \quad (4)$$

The key advantages of using this Dirichlet process model-based clustering are that the underlying distribution of  $x_i$ 's and the number of clusters are unknown. Moreover, one can provide an estimate of the expected number of clusters by using Eqn. (4).

For fitting the model, we used  $\alpha = 1.0$  and a flat prior  $G_0 \sim N_6(0, \sigma^2 \mathbf{I})$  with  $\sigma^2 = 1000$ . The initial value of  $\Sigma$ ,  $\Sigma_0$  is obtained as the sample covariance matrix. We applied the iidWCR algorithm for  $B = 1000$  to obtain the estimate of the number of clusters. Three classes were obtained consistent with the results from the K-means technique. In Table 3 the mean values of the parameters with errors are tabulated. The values are consistent with those found from the K-means method. The number of members of cluster II, 892 is somewhat larger than what was found by the K-means method, 622, but considering the different nature and approach of the two techniques, such differences are perhaps expected. In summary, these two independent clustering techniques indicate that there are three classes of GRB with qualitatively similar properties.

### 3. CLASSIFICATION OF GRB WITH KNOWN RED-SHIFT

Although the classification described in the previous section is based on six GRB parameters the segregation of the classes can be visualized using the total fluence,  $F_T$  and the duration,  $T_{90}$ . This is illustrated in Fig (2) which shows  $F_T$  versus  $T_{90}$  for the members of the three clusters obtained using the K-means technique. The Dirichlet process model gives qualitatively similar results. The solid line representing  $T_{90} = 2$  sec, differentiates the members of Cluster I (marked by triangles) with those of Cluster II (marked by filled circles).

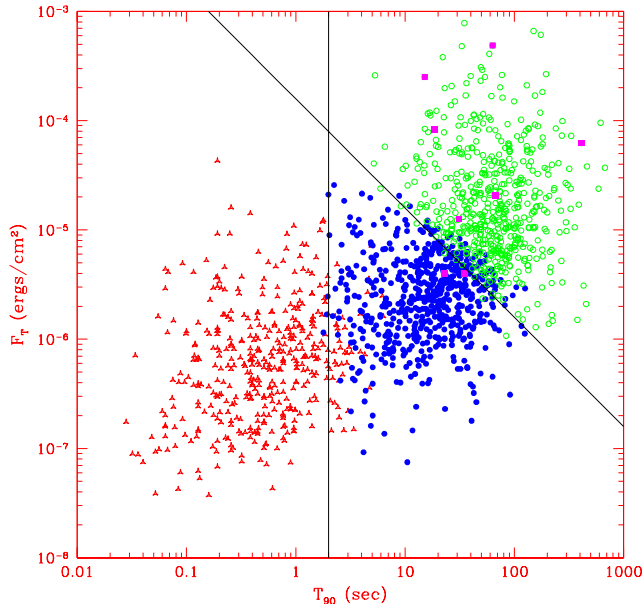


FIG. 2.— The fluence  $F_T$  in  $\text{ergs/cm}^2$  versus the duration  $T_{90}$  in seconds for members of Cluster I (triangles), II (solid circles) and III (open circles) from the K-means clustering method. The solid lines represent  $T_{90} = 2\text{s}$  and  $F_T = 1.6 \times 10^{-4}/T_{90}$   $\text{ergs/cm}^2$  which qualitatively separate the three groups. The solid squares represent eight GRB detected by BATSE for which redshifts are also measured (e.g. Bagoly et al. 2003).

Thus Cluster I is consistent with the standard classification of short duration bursts. The standard long duration bursts (with  $T_{90} > 2\text{ s}$ ) are further classified into two groups with one of them (members of Cluster III, marked using open circles) having typically higher fluence. Thus we have named members of Cluster II and III as low and high fluence GRB. The solid line representing  $F_T = 1.6 \times 10^{-4}/T_{90}$   $\text{ergs/cm}^2$  qualitatively separates two groups. There are eight GRB detected by BATSE for which there are redshift estimates (e.g. Bagoly et al. 2003). These are marked by squares in Figure 2. Six of them are in Cluster III while two are close to the demarking line. One of these GRB (980425) is at a low redshift ( $z = 0.0085$ ) and is associated with a supernova.

To identify a GRB with a known red-shift as a member of a cluster, broad band coverage of the prompt emission is required in order to correctly estimate the total fluence  $F_T$ , which BATSE would have observed for the burst. This is particularly important, when the peak of the energy spectrum of a GRB is at high energies  $> 300\text{ keV}$ . Amati et al. (2002) analyzed GRB with known red-shifts and well constrained spectral parameters over a broad energy range and discovered that the intrinsic (i.e. red-shift corrected) peak of the energy spectrum,  $E_p$  correlates with the isotropic energy output,  $E_{iso}$ . Apart from being a stringent condition and test for any theoretical model that describes the GRB prompt emission, this empirical relation highlights the possibility that GRB can be used to probe and constrain the expansion of the Universe at early times. Ghirlanda et al. (2004) added more GRB to the sample and found that the the beaming corrected luminosity,  $E$  has a tighter correlation with  $E_p$  than the isotropic one. Nevertheless, there is still significant dispersion in the relationship which needs to be explained. In order to see how the

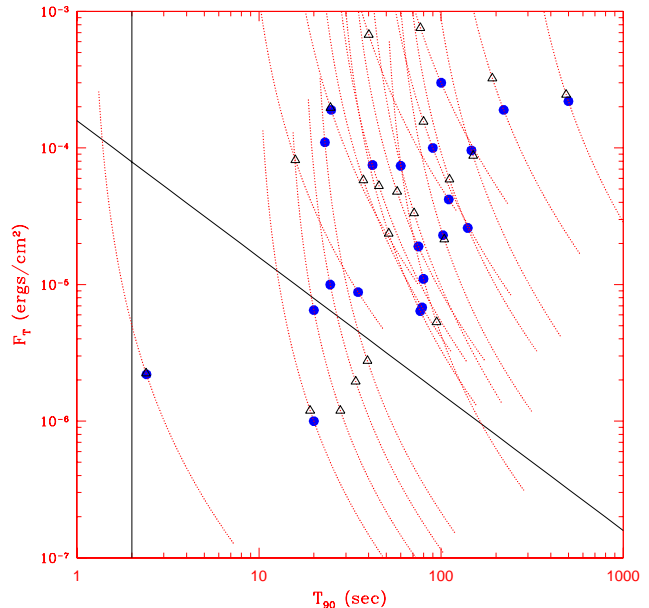


FIG. 3.— The fluence  $F_T$  in  $\text{ergs/cm}^2$  versus the duration  $T_{90}$  in seconds for 21 GRB (filled circles) with known redshifts taken from Ghirlanda et al. (2004) and references therein. The solid lines represent  $T_{90} = 2\text{s}$  and  $F_T = 1.6 \times 10^{-4}/T_{90}$  which qualitatively distinguish the three clusters (Fig 2). For each GRB, the dotted lines represent the predicted fluence and duration if it was located at a redshift range  $0.1 < z < 5$ . The open triangles represent the predicted fluence and duration if the GRB were located at redshift  $z = 1$ . These predicted values allow for the classification of the GRB into members of Cluster II and III.

classification found in this work affects such relationship, we have used 21 GRB listed in Table 1 of Ghirlanda et al. (2004) that have well measured temporal and spectral parameters. The total fluence  $F_T$  versus the duration  $T_{90}$  for these GRB are plotted in Fig. (3) (filled circles). Overlaid on the plot are the two solid lines  $F_T = 1.6 \times 10^{-4}/T_{90}$   $\text{ergs/cm}^2$  and  $T_{90} = 2\text{s}$  which qualitatively segregate the three clusters (Fig 2). Most of the GRB have high fluence and are of long duration (consistent with them being members of Cluster III) which is probably a selection effect. Two of the GRB have  $F_T < 1.6 \times 10^{-4}/T_{90}$   $\text{ergs/cm}^2$  and are probably members of Cluster II. However, there are three GRB with  $F_T \sim 1.6 \times 10^{-4}/T_{90}$   $\text{ergs/cm}^2$  and hence there is an ambiguity about their classification. For each GRB, a corresponding dotted line is plotted in Fig (3) which shows the variation of the observed  $F_T$  versus  $T_{90}$  if the same GRB was located at different red-shifts. The lines are drawn for a red-shift range  $0.1 < z < 5.0$  for a  $\Lambda$  CDM cosmology with  $\Omega_\Lambda = 0.7$  and Hubble parameter  $H = 65\text{ km/s/Mpc}$ . It is interesting to note that the red-shift trajectories for the high fluence GRB in general do not cross the  $F_T = 1.6 \times 10^{-4}/T_{90}$  line. In other words, if these GRB were located at a wide range of red-shifts, their observed fluence would have been  $F_T > 1.6 \times 10^{-4}/T_{90}$  and hence they would have been classified as members of Cluster III. On the other hand there are six GRB whose red-shift trajectories mostly lie below the de-marking line. Their observed fluence would be  $F_T < 1.6 \times 10^{-4}/T_{90}$  for a wide range of red-shifts and hence they would be classified as members of Cluster II. The open triangles in the Figure mark the positions of the GRBs if they were all located at a red-shift,  $z = 1.0$ . In this rep-



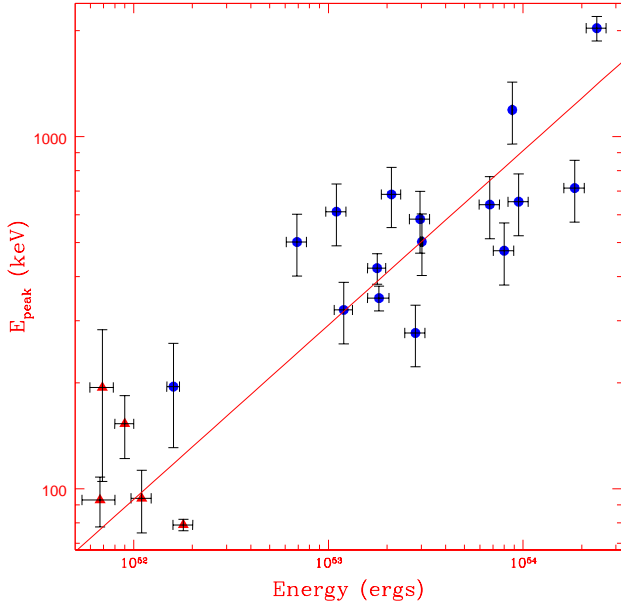


FIG. 4.— The intrinsic (red-shift corrected) peak of the energy flux,  $E_{peak}$  versus the isotropic energy output for 21 GRB with well defined spectral parameters (Amati et al. 2002; Ghirlanda et al. 2004). GRB that are members of Cluster II (triangles) have isotropic energy output of nearly  $10^{52}$  ergs, while members of Cluster III (circles) have a much wider range of energy output.

resentation, the GRB are more clearly segregated into Clusters II and III with five of them having a predicted fluence less than  $F_T > 1.6 \times 10^{-4}/T_{90}$  with the others being significantly brighter. This strongly suggests that the classification described in this work is not due to observational bias arising from the use of observed parameters instead of intrinsic ones.

We classify the 21 GRB according to their predicted observed fluence and duration if they were situated at  $z = 1$ . In this scheme, five GRBs are classified as members of Cluster II while the remaining 18 are identified as members of Cluster III. Fig (4) shows the variation of the intrinsic energy peak  $E_{peak}$  versus the isotropic energy realized,  $E_{iso}$ , which is the correlation discovered by Amati et al. (2002). GRB identified as Cluster I are marked as triangles while those belonging to Cluster III are represented by filled circles. GRB belonging to Cluster II all have an isotropic energy output close to  $\sim 10^{52}$  ergs, while those belonging to Cluster III span a much larger range of energy  $10^{52-54}$  ergs and roughly follow the  $E_p - E_{iso}$  correlation. Although the number of GRB in this sample is small, this segregation of the GRB in intrinsic parameter space is a another indication that the classification is robust and perhaps not due to observational bias. Most of the members of Cluster III have a rest frame peak energy  $E_{peak} > 300$  keV and hence would have had significant flux in the highest energy channel of BATSE, i.e.  $F_4$ . Thus, the retention of  $F_4$  in the classification analysis of §2 is important even though there is systematic uncertainty in the measured value of the fluence. Indeed, if  $F_4$  is not taken into account the evidence for three clusters in the BATSE sample decreases.

#### 4. SUMMARY AND DISCUSSION

Two multivariate clustering techniques, the K-means partitioning method and the Dirichlet process of mixture mod-

eling, have been applied for the first time to the BATSE Gamma-ray burst (GRB) catalog. These two schemes do not make any a priori assumptions about the number of clusters, but instead provide quantitative estimate of the optimal number of groups. The jump curve for the K-means partitioning method suggests that this optimal number is three which is further supported with the value of the expected number of clusters,  $E\{n(p)\}$ , obtained using Dirichlet process of mixture modeling. The two techniques group the GRBs in qualitatively similar classes, which can be described as short bursts ( $T_{90} < 2$  s, Cluster I), long duration, low fluence bursts ( $F_T < 1.6 \times 10^{-4}/T_{90}$  ergs/cm<sup>2</sup>, Cluster II) and long duration, high fluence bursts ( $F_T > 1.6 \times 10^{-4}/T_{90}$  ergs/cm<sup>2</sup>, Cluster III).

To estimate how such a classification, based on observed spectral and temporal parameters, can arise from intrinsic GRB properties, a sample of 21 GRB with known red-shifts and well constrained spectral parameters, are classified within this scheme. The observed total fluence,  $F_T$  and duration  $T_{90}$  for these GRBs if they were located at different red-shifts ( $0.1 < z < 5$ ) were estimated. For 16 of the 21 GRB, the estimated fluence would have satisfied  $F_T > 1.6 \times 10^{-4}/T_{90}$  ergs/cm<sup>2</sup> for nearly the entire range of red-shift space and hence they were classified as high fluence bursts. This invariance in red-shift, indicates that the classification scheme is not strongly effected by observational bias and by the use of observed parameters instead of intrinsic ones. For five GRB, classified as low fluence bursts, the predicted fluence  $F_T < 1.6 \times 10^{-4}/T_{90}$  for a significant fraction of the red-shift space, which again signifies the physical nature of the classification. Based on the classification of these GRB with known red-shift, it can be inferred that the low fluence GRB have a nearly constant isotropic Energy output of  $10^{52}$  ergs and have an intrinsic (red-shift corrected) duration of  $T_{90} \sim 2-30$  secs. On the other hand, the high fluence GRB (Cluster III) have a much wider range of isotropic energy output  $10^{52-54}$  ergs and a corresponding wide range of intrinsic durations 10 - 500 secs.

We note with caution that the number of GRB with known red-shifts, used for this analysis is small and a much larger sample is required before concrete conclusions can be drawn. It is also important, for this analysis, to have well constrained spectral parameters of these GRB. In particular, the peak of the energy fluxes,  $E_p$  are required to be well estimated and since for high energetic sources  $E_p > 300$  keV, it is imperative to have well calibrated high energy information. Indeed, if the highest energy channel of the BATSE measurement is not taken into account, the significance of the classification is smaller.

The classification presented here, needs to be supported by theoretical considerations. It is tempting to identify the low fluence GRB with neutron star-white dwarf mergers (King et al. 2007) and the higher fluences ones with massive stellar collapse. The near constancy of the isotropic energy output of low fluence bursts, seem to be consistent with them being neutron star-white dwarf mergers. Since both neutron stars and white dwarfs do not have significant mass variations, their initial conditions for the binary merger could be similar, leading to the nearly constant energy output. Moreover, their merger time may also be typically smaller than massive stellar collapse time-scales, which is consistent with the shorter intrinsic duration 2–30 s, found in this work. On the other hand, the energy output and duration of GRB induced by

massive stellar collapse may depend on the mass and size of the progenitor which is consistent with the variation inferred for high fluence bursts. The present observational evidence for such a model is not clear. Evidence for supernova light curves have been detected in GRB with different energy output, including some low luminosity ones, e.g. GRB 0311203,  $E \sim 3 \times 10^{49}$  ergs (Malesani et al. 2004), the nearby GRB 060614, for which no supernova was detected also had a low isotropic energy output of  $10^{51}$  ergs. Such low energy output are not represented in the 21 GRB with well constrained spectral parameters used in this analysis which all have energies  $> 10^{52}$  ergs. These rare GRB (since they have to be located relatively nearby to be detected) may not represent a signifi-

cant fraction of the BATSE catalogue. BATSE did detect GRB 980425 which is at low redshift ( $z = 0.0086$ ) and is associated with a supernova. At this redshift, the GRB would be a borderline case between the high and low fluence GRB (Figure 2). Thus the interpretation of the two different classes of long bursts as being due to stellar collapse and white dwarf-neutron star mergers, is speculative and more quantitative theoretical predictions and observational evidences are required before a definite conclusion can be made.

TC and AKC thank the IUCAA associateship program for support

#### REFERENCES

- Amati, L., et al. 2002, *A&A*, 390, 81  
 Bagoly, Z., Meszaros, A., Horvath, I., Balazs, L. G., & Meszaros, P. 1998, *ApJ*, 498, 342  
 Bagoly, Z., Csabai, I., Mészáros, A., Mészáros, P., Horváth, I., Balázs, L. G., & Vavrek, R. 2003, *A&A*, 398, 919  
 Balastegui, A., Ruiz-Lapuente, P., & Canal, R. 2001, *MNRAS*, 328, 283  
 Baumgart, C.W. 1994, in *SPIE Proc. 2243, Applications of Artificial Neural Networks V*, eds. S. K. Rogers & D. W. Ruck (Bellingham: SPIE), 552.  
 Blackwell, D. & MacQueen, J. B. 1973, *Annals of Statistics*, 1, 353.  
 Bloom, J. S., et al. 2006, *ApJ*, 638, 354  
 Dezalay, J.-P., Barat, C., Talon, R., Syunyaev, R., Terekhov, O., & Kuznetsov, A. 1992, *American Institute of Physics Conference Series*, 265, 304  
 Escobar, M. D. & West, M. 1995, *Journal of the American Statistical Association*, 90, 577.  
 Feigelson, E. D., & Babu, G. J. 1998, *IAU Symp. 179: New Horizons from Multi-Wavelength Sky Surveys*, 179, 363  
 Fynbo, J. P. U., et al. 2006, *Nature*, 444, 1047  
 Gehrels, N., et al. 2005, *Nature*, 437, 851  
 Gehrels, N., et al. 2006, *Nature*, 444, 1044  
 Ghirlanda, G., Ghisellini, G., & Lazzati, D. 2004, *ApJ*, 616, 331  
 Hakkila, J., Haglin, D. J., Pendleton, G. N., Mallozzi, R. S., Meegan, C. A., & Roiger, R. J. 2000, *ApJ*, 538, 165  
 Hakkila, J., Giblin, T. W., Roiger, R. J., Haglin, D. J., Paciesas, W. S., & Meegan, C. A. 2003, *ApJ*, 582, 320  
 Hartigan, J. A. 1975, *Clustering Algorithms*, New York, Wiley.  
 Horváth, I. 1998, *ApJ*, 508, 757  
 Horváth, I. 2002, *A&A*, 392, 791  
 Horváth, I., Balázs, L. G., Bagoly, Z., Ryde, F., & Mészáros, A. 2006, *A&A*, 447, 23  
 Ishwaran, H. & Takahara, G., 2002, *Journal of the American Statistical Association*, 97, 1154.  
 Johnson, R. A., & Wichern, D.W. 1996, *Applied Multivariate Statistical Analysis*, Prentice Hall of India.  
 King, A., Olsson, E., & Davies, M. B. 2007, *MNRAS*, 374, L34.  
 Kouveliotou, C., Meegan, C. A., Fishman, G. J., Bhat, N. P., Briggs, M. S., Koshut, T. M., Paciesas, W. S., & Pendleton, G. N. 1993, *ApJ*, 413, L101  
 MacQueen, J., 1967, *Fifth Berkeley Symp. Math. Statist. Prob.*, 1, 281.  
 Malesani, D., et al. 2004, *ApJ*, 609, L5  
 Mukherjee, S., Feigelson, E. D., Jogesh Babu, G., Murtagh, F., Fraley, C., & Raftery, A. 1998, *ApJ*, 508, 314  
 Piran, T. 1992, *ApJ*, 389, L45  
 Piran, T. 2005, *Reviews of Modern Physics*, 76, 1143  
 Sazonov, S. Y., Lutovinov, A. A., & Sunyaev, R. A. 2004, *Nature*, 430, 646  
 Schaefer, B. E., & Xiao, L. 2006, *ArXiv Astrophysics e-prints*, arXiv:astro-ph/0608441  
 Sugar, A. S., & James, G. M. 2003, *JASA*, 98, 750.  
 Soderberg, A. M., et al. 2004, *Nature*, 430, 648  
 Woosley, S. E., & Bloom, J. S. 2006, *ARA&A*, 44, 507